Influence of Iodine Doping on the Structural and Electronic Properties of $CsSnBr_3$

DILSHOD NEMATOV [1,2,*]

[1] S.U.Umarov Physical -Technical Institute of National Academy of Sciences of Tajikistan
[2] M.S.Osimi Tajik Technical University, Dushanbe, 724000 TAJIKISTAN

Abstract: In this work, by means of quantum-chemical calculations within the framework of density functional theory, the considered several structural and electronic properties of nanocrystals of the CsSnBr3−xIx (0≤x≤3) and discussed the effect of iodine concentration on the geometry and electronic properties of these materials. The exchange-correlation effects of electrons were taken into account by the LDA, GGA, and the modified Becke-Jones exchange-correlation potential (mBJ). The results obtained in the framework of the DFT-mBJ and the Wien2k package are in good agreement with the data from experimental measurements and open up the possibility of accurately predicting a number of fundamental properties of perovskite-like complex structures and the development of new materials.

Keywords: density functional theory; band gap; electronic structure; perovskite; Wien2k package.
Received: June 19, 2021. Revised: April 26, 2022. Accepted: June 15, 2022. Published: July 29, 2022.

1. Introduction

The possibilities of converting solar energy and other unconventional forms of energy into electricity are considered in the context of projected global energy needs for the 21st century [1-3]. Therefore, a very urgent task facing scientists and engineers today is the study of several electronic, optical, thermal, and other characteristics of new materials with the aim of their application in solar energy. Furthermore, to successfully transition from fossil fuels to renewable energies, confront climate change, and end pollution, we can no longer rely solely on existing materials but must focus on synthesizing other classes of materials with improved properties. Moreover, the energy demand constantly increases with population growth, and the gap between demand and supply also widens over time [1-3].

Conventional energy production methods will no longer be able to meet the world's energy needs. Therefore, unconventional measures, including the creation of photovoltaic devices, wind farms, and moisture-to-electricity converters, are of great interest, and for the implementation of these tasks and the transition to Green Energy, countries of the world allocate a huge amount of money and support scientists and engineers to strengthen their research works [1].

The effect of converting light into electricity was discovered back in 1839 by Alexander Edmond Becquerel, after which Charles Frits and Jacamo Luigi made the first attempt to create the first light-to-electricity converter. However, this unique discovery did not attract the attention of researchers due to the then low coefficient transformation. Over the years, attempts have been made to increase the photoelectric conversion factor of solar cells, which were created on the basis of silicon, gallium arsenide, and other semiconductor materials. As a tradition for creating solar cells, silicon composites have been widely used due to their unique electrophysical properties, such as bandgap and light absorption capacity. However, at the moment, the maximum conversion efficiency of commercially available silicon converters is only 14-15% [2]. Moreover, the technology for the production of traditional silicon-based solar cells is advanced, but some problems such as high cost and environmental pollution need to be addressed.

In 2013, Science magazine reported on the possibility of using perovskites in solar cells [3]. According to the National Laboratory for Renewable Energy Sources (NREL), perovskites are also widely used in memory devices, LEDs, diodes for ultra-high-power lasers, etc. [4], due to their low cost, high

absorption coefficient, high mobility of charge carriers, composite flexibility, high stability, and adjustable material structure. The only natural perovskite, calcium titanate ($CaTiO_3$), was discovered by Gustav Rose in 1839 and was named perovskite in honor of Count L.A. Perovsky. Later, the artificial synthesis of these structures began with the general formula ABX_3, where X = F^-, Cl^-, Br^-, I^-, and O^{2-}. Elements A and B are two cations of different sizes.

Features and prospects of the use of halide-based perovskites are that it can be tuned either by changing the content of halides or by using the size of the cations to obtain the optimal bandgap for photovoltaic applications. Moreover, the efficiency of perovskite panels is practically already exceeded by 26.7% [5]. However, despite the rapid progress made over the past few years in terms of conversion efficiency, understanding the fundamental properties of perovskites is rather limited. Proceeding from this, the aim of this work is a quantum-chemical study of the geometric and electronic properties of I-doped perovskite nanostructures based on $CsSnBr_3$ in order to find the regularity of the change in their properties under the influence of iodine concentration, as well as to reveal the expediency of further experimental study of the properties of these nanocrystals.

2. Materials and Methods

Ab initio quantum-chemical calculations within the framework of the density functional theory [6] were implemented in the Wien2k package [7]. The DFT is a method based on *ab initio* calculation initially proposed by Hohenberg [8], Kohn, and Sham [9], which has the advantage of not relying on any experimental parameter. The idea of this method is to replace the interacting electronic system by a fictitious non-interacting electronic system that gives the same electronic density as the interacting system. The XC potential affecting the non-interacting electronic system can be obtained from the XC energy, which is only a function of the electronic density. However, no exact functional exists, but many approximative functionals have been developed, for example, LDA, GGA. The object under study was the orthorhombic structures of nanocrystals of the $CsSnBr_{3-x}I_x$ ($0 \le x \le 3$) family (systems $CsSnBr_3$, $CsSnBr_2I$, $CsSnBrI_2$ и $CsSnI_3$). The radius of the Mufftin sphere (RMT) for Cs, Sn, and I was taken as $2.5a_0$, and for Br - $2.07a_0$, where a_0 is the Bohr radius. Nevertheless, the crystal structures of the materials under study are shown in Figure 1.

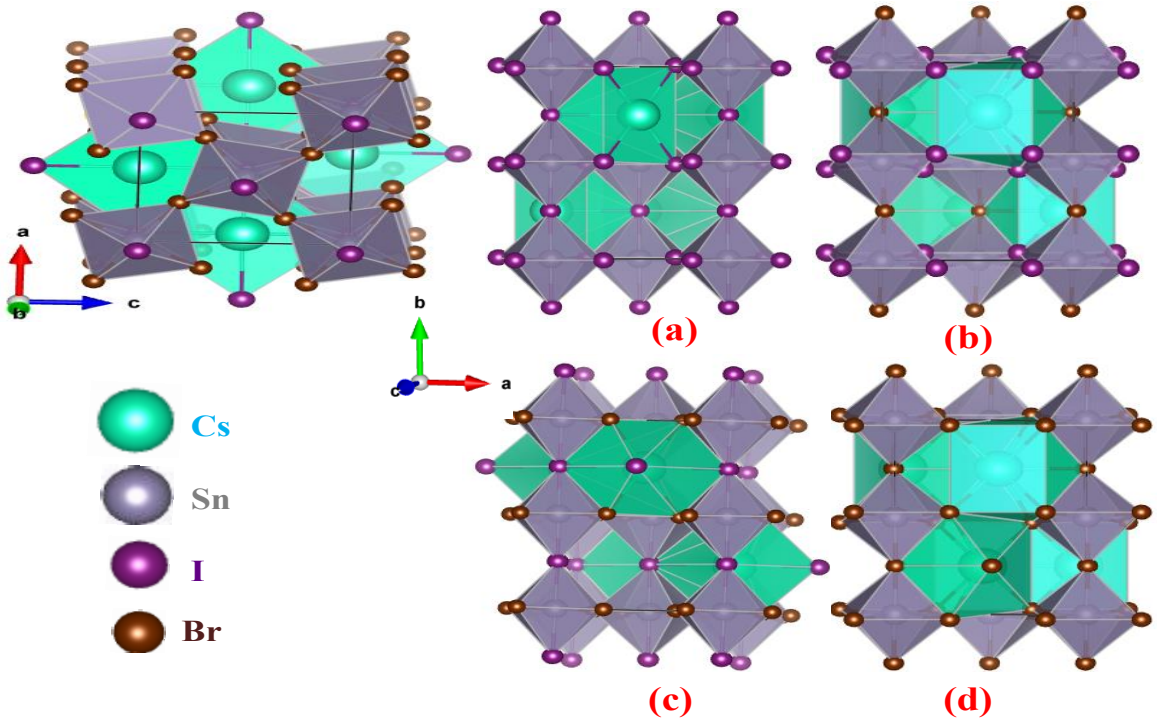

Figure 1. Schematic illustration of crystal structures of **(a)** $CsSnBr_3$, **(b)** $CsSnBr_2I$, **(c)** $CsSnBrI_2$ and **(d)** $CsSnI_3$.

The valence wave functions inside the MT sphere were expanded to lmax = 10, and the charge density was expanded in a Fourier series up to Gmax. For sufficiently good convergence in the parameters of the total crystal lattice energy, all atomic geometry optimizations for the orthorhombic unit cell of $CsSnBr_{3-x}I_x$ system were performed using k-points generated by uniform grid parameters 3 × 2 × 3.

In addition to using the LDA and GGA approximations, the study of electronic properties required the use of the modified Becke-Johnson potential (TB-mBJ) [10], the formulation of which is given as follows:

$$E_{xc}^{mBJ}(r) = cE_x^{BR}(r) + (3c-2)\frac{1}{\pi}\sqrt{\frac{5k(r)}{6\rho(r)}} \quad (1),$$

where k (r) is the kinetic energy density according to the Kohn - Sham equation, is the spin-dependent electron density, and E_x^{BR} - is the Becke - Roussel exchange functional (BR). c, is the added parameter by Tran and Blaha to the mBJ potential.

TB-mBJGGA and TBmBJ + LDA potentials, whose mBJ exchange potential is available in the LIBXC interface library [11], are used in combination with lattice parameters optimized by the GGA and LDA approximations.

3. Results and Discussion

3.1. Structural properties.

Determination of the structural specification (optimized lattice constants (a, b, c), volume (V), and angles between a, b and c) is inevitable for describing the structural properties of materials. The equilibrium lattice parameters of the materials under study are determined after optimization, where all these materials have the space group Pnma (62). Equilibrium lattice parameters were obtained by approximating the total energy as a function of the normalized volume, according to the equation of state of the ground state (EOS), the analytical expression of which is determined using the Birch-Murnaghan approximation [12]:

$$E(V) = E_0 + \frac{9}{8}B_0V_0\left[\left(\frac{V_0}{V}\right)^{2/3}-1\right]^2 + \frac{9}{16}B_0(B_0'-4)V_0\left[\left(\frac{V_0}{V}\right)^{2/3}-1\right]^3 \quad (2)$$

where E_0 - is the DFT ground state energy. B_0 – bulk modulus, B_0' - pressure derivative of the volumetric modulus ($B'=(\partial B/\partial P)T$), V-is the volume of the cell, V_0-equilibrium volume, that is, when the system is in a relaxing (ground) state.

The calculated optimized lattice parameters (a, b, c, and V) and bond lengths for all structures are shown in Table 1, and the experimental data are compared.

Table 1. Comparison of calculated structural parameters with experimental ones.

$CsSnBr_{3-x}I_x$		$CsSnBr_3$	$CsSnBr_2I$	$CsSnBrI_2$	$CsSnI_3$
Lattice parameters, Å	This work	a = 8.3557 b = 11.730 c = 8.2055	a = 8.2064 b = 12.619 c = 8.2046	a = 8.4670 b = 12.551 c = 8.4675	a = 8.9081 b = 12.435 c = 8.4355
	Exp.	a= 8.3634 [13] b=11.760 [13] c=8.1782 [13]	-	-	a= 8.688 [14] b= 12.37 [14] c= 8.643 [14]
Volume, $Å^3$	This work	804.2926	849.6717	899.9003	934.4653
	Exp.	804.4168 [13]	-	-	929.4687 [14]

Comparison of the tabular data indicates that the calculated structural parameters for the unbiased systems $CsSnBr_3$ and $CsSnI_3$ are in good correlation with the experimental results (Table 1). However, there are no experimental data in the literature on comparing the lattice parameters of mixed perovskites $CsSnBr_2I$ and $CsSnBrI_2$.

Further, Figure 2 shows the dependences of the volume of nanocrystals of the $CsSnBr_{3-x}I_x$ ($0 \le x \le 3$) system on the iodine concentration.

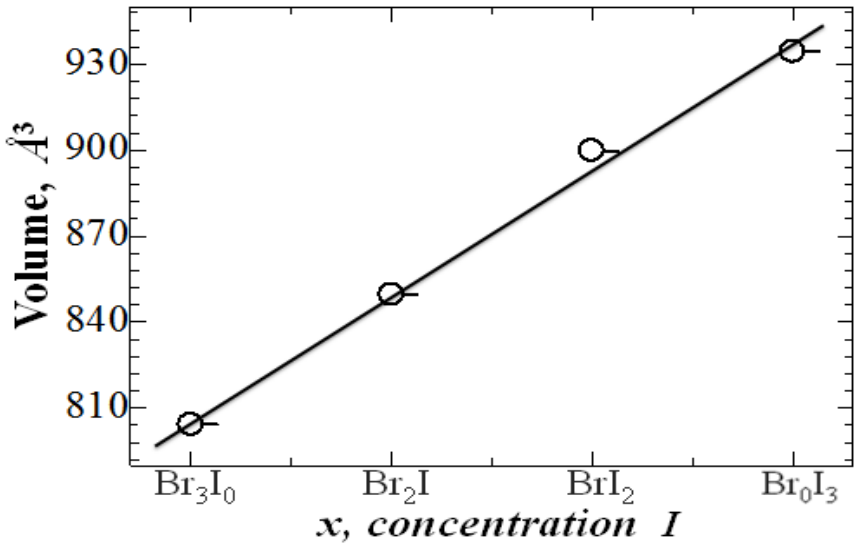

Figure 2. Change in the volume of the $CsSnBr_{3-x}I_x$ system depending on the Br/I ratio. Volume as a function of iodine concentration (x).

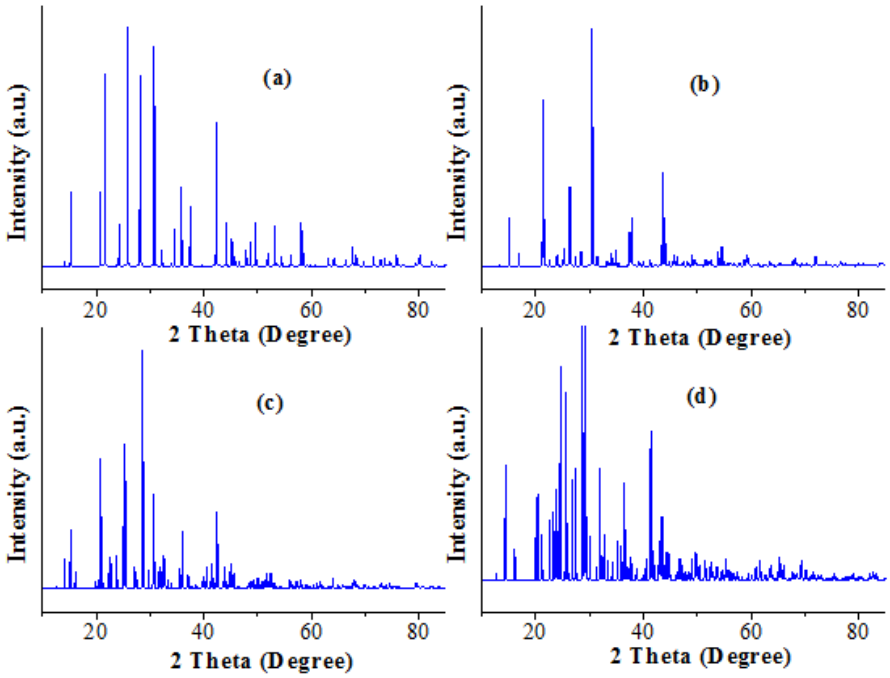

Figure 3. Theoretical powder diffractograms of **(a)** $CsSnBr_3$, **(b)** $CsSnBr_2I$, **(c)** $CsSnBrI_2$; **(d)** $CsSnI_3$.

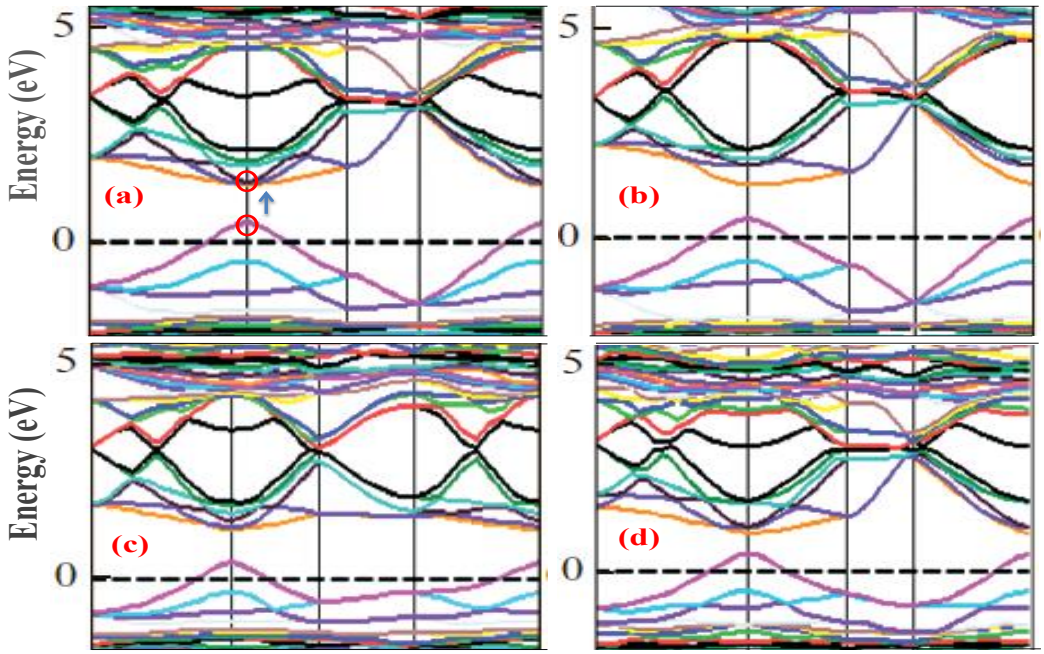

Figure 4. Electronic band structures of **(a)** $CsSnBr_3$, **(b)** $CsSnBr_2I$, **(c)** $CsSnBrI_2$ and **(d)** $CsSnI_3$.

From the results obtained, listed in Table 1 and Figure 2, it can be noted that as the transition from $CsSnBr_3$ to $CsSnI_3$, that is, with an increase in the iodine concentration in the system, the volume of these nanocrystals increases linearly, which obeys Vegard's law.

Figure 3 (a-d) shows the X-ray diffraction patterns obtained from the optimized geometries of the studied materials, which were taken using the REFLEX program included in the Materials Studio software package, with CuKa radiation with a wavelength λ = 1.54 Å. According to the results, with an increase in the concentration of iodine in the system, the densification of X-ray peaks is observed and, accordingly, their shift towards small angles.

According to the results, the lattice constants we calculated for these materials are in good agreement with the experimental data (in all cases, less than 1%) [13, 14], which testifies and confirms the correctness of the steps for optimizing the volume and, accordingly, the reliability of our calculations during further quantum-chemical analysis. Calculations of the electronic properties of these materials.

3.2. Electronic properties.

Calculations of the optimized structures' electronic properties were based on density functional theory (DFT) using the Wien2k package. The exchange and correlation effects of electrons were taken into account by the exchange-correlation functionals LDA, GGA, and mBJ, within which different values of the bandgap were obtained for nanocrystals of the $CsSnBr_{3-x}I_x$ system.

The band structure diagram tells us whether the material has a direct or indirect bandgap in addition to the bandgap value. Furthermore, it also tells us about the p-type, n-type or intrinsic nature of the semiconducting materials based on the position of the Fermi level. Our results showed that the minima of the conduction band and the maxima of the valence band of all materials under study are located at the point Γ and indicate a high symmetry (Figure 4), which indicates direct interband transitions in semiconductors, which is very favorable for light absorption. For pure cesium iodide, there is a band inversion at the point Γ, as reported in topological insulators. This phenomenon has been discussed in previous reports on other

halide perovskites [15, 16]. The Fermi level is set to 0 for all band structures.

As a rule, GGA and LDA significantly underestimate the bandgap and band structure. Therefore, in the tabular results and graphical dependencies presented in this work, particularly band structures and density of states, only the results of mBJ calculations are given since numerous studies have confirmed the suitability of the mBJ functional for bandgap estimates [17-28].

Because of the importance of iodides in photovoltaic applications, it is important to calculate as accurately as possible the parameters of the electronic structure of the systems under study, especially the bandgap. The calculated band gaps are given in Table 2, from which it can be seen that the values of the bandgap by the modified TB-mBJ functional are much more similar to the experiment as compared to GGA and LDA.

Table 2. Comparison of the calculation results of the band-gap with the literature data.

$CsSnBr_{3-x}I_x$			**$CsSnBr_3$**	**$CsSnBr_2I$**	**$CsSnBrI_2$**	**$CsSnI_3$**
Bandgap, eV	this work	LDA	0.91	0.82	0.73	0.61
		GGA	0.89	0.67	0.61	0.58
		mBJ	1.725	1.635	1.486	1.307
	experiment		1.720[29]	-	-	1.30 [30]
	other calculations		1.01 [31]	-	-	0.885 [32], 1.71[33]

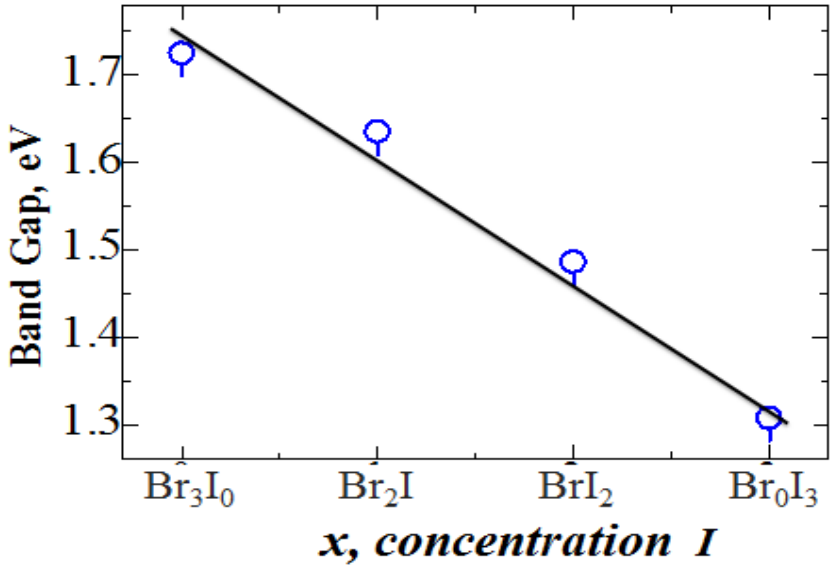

Figure 5. Calculated band-gap as a function of Br concentration for $CsSnBr_{3-x}I_x$ system.

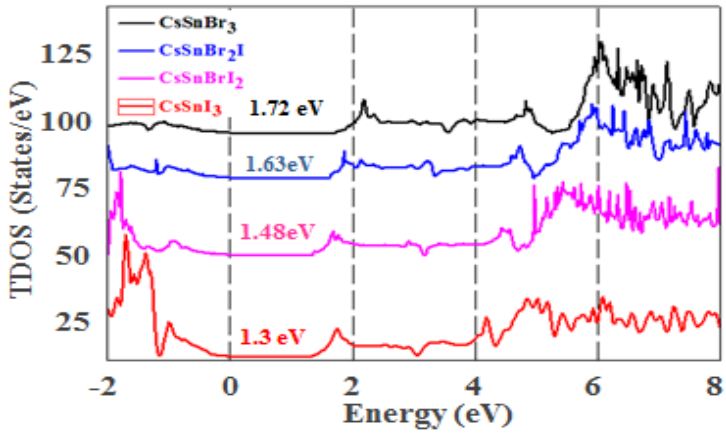

Figure 6. Total density of states for **(a)** $CsSnBr_3$, **(b)** $CsSnBr_2I$, **(c)** $CsSnBrI_2$, **(d)** $CsSnI_3$.

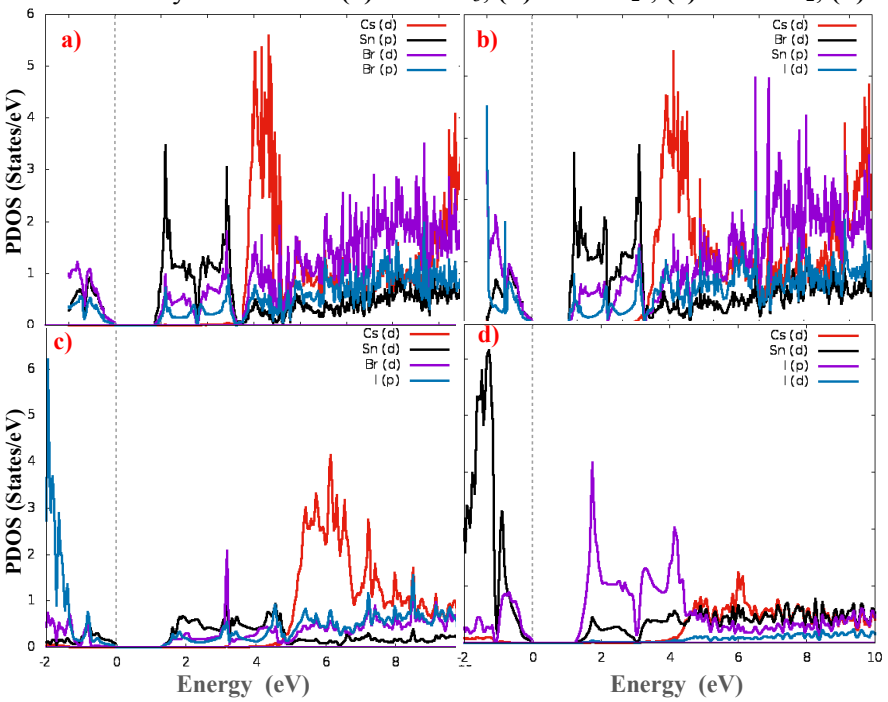

Figure 7. Partial density of states for **(a)** $CsSnBr_3$, **(b) $CsSnBr_2I$, (c)** $CsSnBrI_2$**, (d)** $CsSnI_3$.

The values of the bandgap obtained by us for $CsSnBr_3$ and $CsSnI_3$ correspond with high accuracy to the literature data, especially the results of experimental measurements. However, for displaced perovskites ($CsSnBr_2I$ and $CsSnBrI_2$), there are no data for comparisons in the literature. Figure 5 shows the graphs of the change in the bandgap of the $CsSnBr_{3-x}I_x$ system depending on the concentration of iodine doping.

As shown in Figure 5, as the iodine concentration increases, the bandgap decreases linearly; that is, by controlling the iodine content, the bandgap can be adjusted to approach the optimal bandgap.

Either way, the electronic properties of materials are based on the bandgap, which lies in the density of electronic states (DOS). Therefore, understanding its formation becomes vital for the design and manufacture of optoelectronic devices. Figure 6 shows the total density of states (TDOS) for all members of the $CsSnBr_{3-x}I_x$ system as a function of the bandgap. The Fermi level is set to 0.

The enhanced density of states for the $CsSnI_3$ and $CsSnIBr_2$ systems means that with an increase in the iodine concentration in the system, the vacancy level in the outer orbitals increases, and many places will be available for occupation.

The electronic structures of materials near the top of the valence band and the bottom of the conduction band are of vital importance for their electronic transport properties [34–38]. Accordingly, partial densities of states (PDOS) were calculated for the materials under study, which estimate the contribution of each atom and specific electronic states to the formation of the valence and conduction bands near the Fermi level (Figure 7).

The PDOS plots can be explained by two aspects: orbitals, which contribute near the band edges, and the general contribution of states. In the $CsSnBr_3$ system, electrons of the I (d) -state and Sn (p) -state contribute near the valence band (CB) and conduction bands (CB), respectively (Figure 7 (a)). The general contributions to the formation of VB are mainly made by the p-state of Sn and I and Cs (d) to CB. In the case of $CsSnBr_2I$, an insignificant contribution is made by electrons of all types of atoms (except for Cs) near the VB edge (Figure 7 (b)). There are also small contributions from Cs (d), I (d), Sn (p), and Br (d) — states at the meeting point of VB and CB. In the formation of electronic states of

$CsSnBrI_2$ near the band edges, the contribution is made by the I (p), Br (d), and Sn (d) state (Figure 7 (c)). However, the d-states of Cs electrons have the maximum contribution in the upper part of the CB. The results show that the I (d) and Sn (d) orbitals make the main contribution to the formation of allowed bands (near the band edges) and to the overall contribution of the states of the conduction band $CsSnI_3$. There is also a significant contribution from the d-electrons of the Cs atoms (Figure 7 (d)).

Thus, our results can contribute to understanding some of the features of their optical properties, which are important for the practical application of the studied systems. They may be of interest for researchers searching for materials with predetermined and programmed optoelectronic properties [39–45].

4. Conclusions

The structural and electronic properties of displaced perovskite nanocrystals $CsSnBr_3$, $CsSnIBr_2$, $CsSnI_2Br$, and $CsSnI_3$ were studied in work with the implementation of quantum-chemical calculations. It was found that the bandgap decreases linearly with increasing iodine concentration and approaches the optimal band gap for photovoltaic applications.

The results obtained can be used by other researchers to model the structure of substances expected to be synthesized, as well as to determine such an important component as "composition-structure-property".

References

[1]. Gielen, D.; Boshell, F.; Saygin, D.; Bazilian, M. D.; Wagner, N.; Gorini, R. The role of renewable energy in the global energy transformation. Energy Strategy Reviews 2019, 24, 38-50, https://doi.org/10.1016/j.esr.2019.01.006.

[2]. Linghai, M.; Xian-Gang, W.; Sai, M.; Lifu, Sh.; Mengjiao, Zh.; Lingxue,W.; Yu, Ch.; Qi, Chen.; Haizheng, Zh. Improving the efficiency of silicon solar cells using *in situ* fabricated perovskite quantum dots as luminescence downshifting materials. *Nanophotonics* **2019**, *9* , 93-100, https://doi.org/10.1515/nanoph-2019-0320.

[3]. Coontz Robert. Science's Top 10 Breakthroughs of 2013.*Science* **2013**, https://www.science.org/content/article/sciences-top-10-breakthroughs-2013.

[4]. Afsari, M.; Buchani, A.; Khantezade, M. Electronic, optical and elastic properties of the cubic perovskite $CsPbI_3$: based on the study of first principles. *Optik - International Journal for Light and Electron Optics* **2016**, *127*, 12733–12743, https://doi.org/10.1016/J.IJLEO.2016.09.013.

[5]. Yoshikawa, K. Silicon heterojunction solar cell with colliding reverse contacts for photoconversion efficiency over 26%. *Nature Energy* **2017**, *2*, 17032, https://doi.org/10.1038/nenergy.2017.32.

[6]. Parr, R. G.; Yang, W. Density-Functional Theory of Atoms and Molecules. *New York: Oxford University Press* **1989**, https://doi.org/10.1093/oso/9780195092769.001.0001.

[7]. Blaha, P.; Schwarz, K.; Tran, F.; Laskowski, R.; K, H.; Madsen, G; D, Marks. Laurence."WIEN2k: An APW+lo program for calculating the properties of solids. *Journal of Chemical Physics* **2021**, *152*, 074101, https://doi:10.1063/1.5143061.

[8]. Hohenberg, P.; Kohn, W. Inhomogeneous Electron Gas. *Phys. R.* **1964**, *136*, B864 https://doi.org/10.1103/PhysRev.136.B864.

[9]. Kohn, W.; Sham, L. Self-Consistent Equations Including Exchange and Correlation Effects. *Physical Review A* **1965**, *140*, 1133-1965, https://doi.org/10.1103/PhysRev.140.A1133.

[10]. David, K.; Fabien, T.; Peter, B. Merits and limits of the modified Becke-Johnson exchange potential. *Physical Review B* **2011**, *83*, 195134, https://doi.org/10.1103/PhysRevB.83.195134.

[11]. Marques, A.; Micael, J.; Tobias, B. A library of exchange and correlation functionals for density functional theory. *Comput. Phys. Commun.* **2012**, *183*, 2272, https://doi.org/10.1016/j.cpc.2012.05.007.

[12]. Birch, Francis. Finite elastic strain of cubic crystals. *Phys. Rev.* **1947**, *71*, 809, https://doi.org/10.1103/PhysRev.71.809.

[13]. Kulbak, M. Cesium enhances long-termstability of lead bromide perovskite-based solar cells. *The J.Phys.Chem.Lett.* **2015**, *7*, 167–172, https://doi.org/10.1021/acs.jpclett.5b02597.

[14]. Yamada, K. Structural phase transitions of the polymorphs of $CsSnI_3$ by means of rietveld analysis of the X-ray diffraction. *Phys. Rev.A.* **1991**, *20*, 801-804, https://doi.org/10.1021/acs.inorgchem.0c00958.

[15]. Giorgio, S. Carbon Nanomaterials: Synthesis, Functionalization and Sensing Applications. *Nanomaterials* **2021**, *11,* 967, https://doi.org/10.3390/nano11040967.

[16]. Stanislav, Ch.; Xiaoliang, Q.; Kübler, Z. Tunable multifunctional topological insulators in ternary Heusler compounds. *Nature Materials* **2010**, *9*, 541-545, https://doi.org/10.1038/nmat2770.

[17]. Nematov, D. D.; Khusenzoda, M. A.; Burhonzoda, A.S.; Kholmurodov, Kh.T.; Lyubchyk, A.; Medhat I. Investigation of Structural and Optoelectronic Properties of N-Doped Hexagonal Phases of TiO_2 ($TiO_{2-x}N_x$) Nanoparticles with DFT Realization: OPTIMIZATION of the Band Gap and Optical Properties for Visible-Light Absorption and Photovoltaic Applications. *Biointerface research in applied chemistry* **2021**, *12*, 3836 – 3848, https://doi.org/10.33263/BRIAC123.38363848.

[18]. Nematov, D.D. Computer analysis of the electronic and structural properties of $CsSnI_3$:Cl and $CsPbI_3$:Cl nanocrystals [Нематов, Д. Компьютерный анализ электронных и структурных свойств нанокристаллов $CsSnI_3$:Cl и $CsPbI_3$:Cl]. *SCI-ARTICLE.RU* **2019**, *76*, 187-196, https://sci-article.ru/stat.php?i=1577288854.

[19]. Doroshkevich, A.; Nabiev, A.; et all. Frequency Modulation of the Raman Spectrum at The Interface DNA-ZrO_2 Nanoparticles. *Egyptian Journal of Chemistry* ***2019***, *62*, 13-20, https://doi.org/10.21608/ejchem.2019.12898.1806 .

[20]. Nematov, D.; Burkhonzoda, A.; Khusenov, M.; Kholmurodov, Kh.; Doroshkevich, A.; Doroshkevich, N.; Zelenyak, T.; Majumder, S. Molecular Dynamics of DNA Damage and Conformational Behavior on a Zirconium-Dioxide Surface. *Journal of Surface Investigation: X-ray, Synchrotron and Neutron Techniques* **2019**, *13*, 1165–1184, https://doi.org/10.1134/S1027451019060430.

[21]. Nematov, D.; Burkhonzoda, A.; Khusenov, M.; Kholmurodov, Kh.; Doroshkevich, A.; Doroshkevich, N.; Zelenyak, T.; Majumder, S; Ahmed, R.; Medhat, I. Molecular Dynamics Simulations of the DNA Radiation Damage and Conformation Behavior on a Zirconium Dioxide Surface. *Egyptian Journal of Chemistry* **2019**, *62*, 149-161, https://doi.org/10.21608/ejchem.2019.12981.1811.

[22]. Burkhonzoda, A; Giyosov, S.; Nematov, D.; Khusenov, M.; Kholmurodov, H. Quantum-mechanical calculation of the electronic structure of ZrO2:Ti^{4+} in the framework of the density functional theory. [Бурхонзода, А,; Гиёсов, С.; Нематов, Д.; Хусенов, М.; Холмуродов, Х. Кванто-механический расчет электронного строения ZrO_2:Ti^{4+} в рамках теории функционала плотности]. *Polytechnic Bulletin. Series: Intellect. Innovation. Investments [Политехнический вестник. Серия: Интеллект. Инновации. Инвестиции]* **2019**, *3*, 11-17.

[23]. Nematov, D.; Burhonzoda, A.; Khusenov, M.; Kholmurodov, Kh.; Yamamoto, T. First principles analysis of geometrical structure, electronic and optical properties of CsSnI3-xBrx perovskite for photoelectric applications. *Journal of Surface Investigation: X-ray, Synchrotron and Neutron Techniques* **2021**, *15*, 532–536, https://doi.org/10.1134/S1027451021030149.

[24]. Burkhonzoda, A.S.; Nematov, D.D.; Khodzhakhonov, I.T.; Boboshirov, D.I. Optical properties of nanocrystals of the $TiO_{2-x}N_x$ system [Оптические свойства нанокристаллов системы $TiO_{2-x}N_x$]. *SCI-ARTICLE.RU* **2021**, *92*, 176-187, https://sci-article.ru/stat.php?i=1621254426.

[25]. Burkhonzoda, A.S.; Nematov, D.D.; Kholmurodov, Kh.T. Structural and electronic properties of nanoscale thin films based on ZrO_2 [Структурные и электронные свойства наноразмерных тонких плекнок на основе ZrO2], *SCI-ARTICLE.RU* **2021**, *92*, 143-1152, https://sci-article.ru/stat.php?i=1623240070.

[26]. Nematov, D.D. Modeling the impact of ionizing radiation on the process of immobilization of biological molecules [Моделирование воздействия

ионизирующего излучения на процесс иммобилизации биологических молекул]. *SCI-ARTICLE.RU* **2020**, *81*, 12-35, https://core.ac.uk/download/344742895.pdf.

[27]. Nematov, D.D. MD modeling of the processes of interaction and encapsulation of nucleotides in the matrix of a carbon nanotube with gold nanoparticles [МД моделирование процессов взаимодействия и инкапсуляции нуклеотидов в матрице углеродной нанотрубки с наночастицами из золота]. *SCI-ARTICLE.RU* **2020**, *83*, 71-91, https://sci-article.ru/stat.php?i=1593585575.

[28]. Nematov, D.D. Research and optimization of optoelectronic properties of N-doped titanium dioxide ($TiO_{2-x}N_x$) nanoparticles for photovoltaic applications [Исследование и оптимизация оптоэлектронных свойств N-легированных наночастиц диоксида титана ($TiO_{2-x}N_x$) для фотоэлектрических применений]. *SCI-ARTICLE.RU* **2021**, *91*, 110-130, https://sci-article.ru/stat.php?i=1616187629.

[29]. Stephen, J. C.; John, D. D.; Josephine, A. H. Evidence for the direct population of solid-state bands by non-bonding electron pairs in compounds of the type $CsM_{II}X_3$(M_{II}= Ge, Sn, Pb; X = Cl, Br, I) . *J. Mater. Chem.* **1995**, *5*, 1813-1818, https://doi.org/10.1039/JM9950501813.

[30]. Zhuo, Ch.; Jian, J.; Wang, Y. Schottky solar cells based on $CsSnI_3$ thin-films/ *Appl. Phys. Lett.* **2012**, *101*, 093901, https://doi.org/10.1063/1.4748888.

[31]. Atchara, P.; Yongyut, L. Band alignment of cesium-based halide perovskites. *Ceram. Int.* **2018**, *44*, 161−163, https://doi.org/10.1016/j.ceramint.2018.08.124.

[32]. Stephen, J. C.; John, D. D. High-temperature Mössbauer studies on ^{119}Sn-enriched caesium tin(II) chlorides and bromides. *J. Chem. Soc., Dalton Trans.* **1995**, 2723-2727, https://doi.org/10.1039/DT9950002723.

[33]. Borriello, I.; Giovanni, C.; Domenico, N. Ab initio investigation of hybrid organic-inorganic perovskites based on tin halides. *Phys. Rev. B* **2008**, *77*, 235214, https://doi.org/10.1103/PhysRevB.77.235214.

[34]. Tripathy, A.; Behera, M.; Rout, A.S.; Biswal, S.K.; Phule, A.D. Optical, Structural, and Antimicrobial Study of Gold nanoparticles Synthesized Using an Aqueous Extract of Mimusops elengi Raw Fruits. *Biointerface Research in Applied Chemistry* **2021**, *10*, 7085-7096, https://doi:10.33263/briac106.70857096.

[35]. Najm, A.S.; Moria, H.; Ludin, N.A. Areca catechu as photovoltaic sensitizer for dye-sensitized solar cell (DSSC). *Biointerface Research in Applied Chemistry*, **2020**, *10*, 5636-5639, https://doi:10.33263/briac103.636639.

[36]. Mawloud, B.; Norredine, M.; Omar, A.; Aamir, H. Optoelectronic properties of the novel perovskite materials $LiPb(Cl:Br:I)^3$ for enhanced hydrogen production by visible photo-catalytic activity: Theoretical prediction based on empirical formulae and DFT. *International Journal of Hydrogen Energy* **2020**, *45,* 33466-33477, https://doi.org/10.1016/j.ijhydene.2020.09.066.

[37]. Christopher, J.; Christopher, J.; Jacob, M. Inorganic Halide Double Perovskites with Optoelectronic Properties Modulated by Sublattice Mixing. *J. Am. Chem. Soc.* **2021**, *142*, *11*, 5135–5145, https://doi.org/10.1021/jacs.9b12440.

[38]. Gleb, N. Z.; Larisa, A. M.; Tatyana, Y.P.; Larisa, A.S.; Elena, V. Simanina . Inhibition of Adenylate Cyclase of Regeneration-Competent Cells of Nervous Tissue: a Novel Approach for the Treatment of AlcoholicEncephalopathy. *Biointerface Research in Applied Chemistry* **2021**, *12,* 1547–1560, https://doi.org/10.33263/BRIAC122.15471560.

[39]. Maria, C.; Folgueras, M.; C, F.; Jianbo, J.; Mengyu, G.; Li, N. Q.; Julian, A. S.; Shivani, S.; Michael, B.; Ross, R. Z.; Fabian, S.; Kerstin, S-A.; Mark, A.; Peidong, Y Lattice Dynamics and Optoelectronic Properties of Vacancy-Ordered Double Perovskite Cs_2TeX_6 (X = Cl^-, Br^-, I^-) Single Crystals. *J. Phys. Chem. C* **2021**, *125*, 25126–25139, https://doi.org/10.1021/acs.jpcc.1c08332.

[40]. Husein, I.; Rahmawaty, V.; Kinarya, E.; Patonah, N. The effect of photoconductive mole fraction based on thin film $Ba_xSr_{1-x}TiO_3$ (X=0.000; 0.125; 0.250; 0.375; 0.500) on electrical properties and diffusivity coefficient. *Biointerface Research in Applied*

Chemistry, **2021**, *11*, 14956-14963, https://doi.org/10.33263/BRIAC116.1495614963.

[41]. Jingjing, L.; Junle, Q.; Thomas, K.; Jun, S. Optoelectronic devices based on the integration of halide perovskites with silicon-based *materials. J. Mater. Chem. A* **2021**, *9,* 20919-20940, https://doi.org/10.1039/D1TA04527J.

[42]. Bhanu, M.; Venkata, S.; Sriram, M.; Hussen, M.; Syam, S.; Basavaiah, Ch. Photocatalytic Activity of Heavy Metal Doped CdS Nanoparticles Synthesized by Using Ocimum sanctum Leaf Extract. *Biointerface Research in Applied Chemistry* **2021**, *11*, 12547 - 12559, https://doi.org/10.33263/BRIAC115.1254712559.

[43]. Nematov, D. D.; Burhonzoda, A. S.; Khusenov, M. A.; Kholmurodov, K. T.; Ibrahim, M. A. The quantum-chemistry calculations of electronic structure of boron nitride nanocrystals with density Functional theory realization. *Egyptian Journal of Chemistry* **2019**, *62*, 21-27, doi:10.21608/EJCHEM.2019.12879.1805.

[44]. Xiang, G.; Wu, Y.; Li, Y.; Cheng, C.; Leng, J.; Ma, H. Structural and Optoelectronic Properties of Two-Dimensional Ruddlesden–Popper Hybrid Perovskite $CsSnBr_3$. *Nanomaterials*, **2021,** *11*(8), 2119, doi:10.3390/nano11082119.

[45]. Zhang, F.; Ma, Z.; Shi, Z.; Chen, X.; Wu, D.; Li, X.; Shan, C. Recent advances and opportunities of lead-free perovskite nanocrystal for optoelectronic application. *Energy Material Advances* **2021**, *5198145*, doi.org/10.34133/2021/5198145.